Proximity Detection and Ranging Using a Modified Fluorescent Lamp for Security Applications

John Cooley
IEEE Student Member
Massachusetts Institute of Technology
MIT Rm. 10-069
77 Massachusetts Ave.
Cambridge, MA 02139
USA

Al-Thaddeus Avestruz
IEEE Member
MIT
MIT Rm. 10-017
77 Massachusetts Ave.
Cambridge, MA 02139
USA

Steven Leeb
IEEE Senior Member
MIT
MIT Rm. 10-069
77 Massachusetts Ave.
Cambridge, MA 02139
USA

Abstract

This paper describes a proximity detection system that uses a fluorescent lamp as a capacitive sensor. Because of the ubiquity of fluorescent lamps in commercial buildings, public spaces, and households, the potential applications of a capacitive sensor of this nature are numerous. These applications include people counting, real-time people tracking and detection of anomalous objects on a person for security verification.

Modeling simulations and calculations of the electric fields under the lamp in the presence of a person as well as circuitry and electrode setups, which can be used to obtain a practical detection range are presented. Real-time tracking data and outputs collected from a working fluorescent lamp sensor are also presented.

Index Terms

Capacitive Sensor, Fluorescent Lamp, Security, Detection, Low-noise, Proximity, Ranging.

I. Introduction

With the ubiquity of fluorescent lamps in commercial and government buildings, there is an untapped infrastructure in place, which may be exploited for security and surveillance applications. The infrastructure of fluorescent lighting provides electric power, an abundant and controlled electric field source, and potential networking over power line modems. As a first step to exploiting the potential advantages of the fluorescent lamp infrastructure for security and monitoring applications, a lamp was modified to be used as a capacitive sensor. The capacitive sensor uses of the alternating electric field from the fluorescent bulbs to measure how the electric field distorts over time, deducing changes in conductivity and permittivity in the space below the lamp. These measurements can be used over practical ranges to detect the presence or movement of people. These measurements can also potentially be used to differentiate people based on shape, chemical makeup or possession of metallic objects. Integrating the whole infrastructure of lamps in a public space via wireline modems or other communication means could lead to a sophisticated and expansive security tracking system.

To use the fluorescent lamp as a capacitive sensor, two 1 inch-wide metallic electrodes are suspended in front of the lamp and a differential voltage measurement is measured between them as shown in Figure 1. These electrodes could potentially be installed on the inside of the lamp cover with a transparent conductor such as Indium-Tin Oxide [3].

In Section II, a lumped capacitor circuit model for the system consisting of the sensor and target is presented. Section III describes the circuit design and signal conditioning implemented to obtain practical detection ranges of 10 ft. from the lamp. Section IV calculates detection ranges and sensor responses based on the above circuitry and noise floor. Section V describes the physical configuration and practical issues dealt with in modifying the lamp as a capacitive sensor. Finally, Section VI presents data from a working lamp sensor prototype demonstrating practical detection ranges for various electrode configurations.

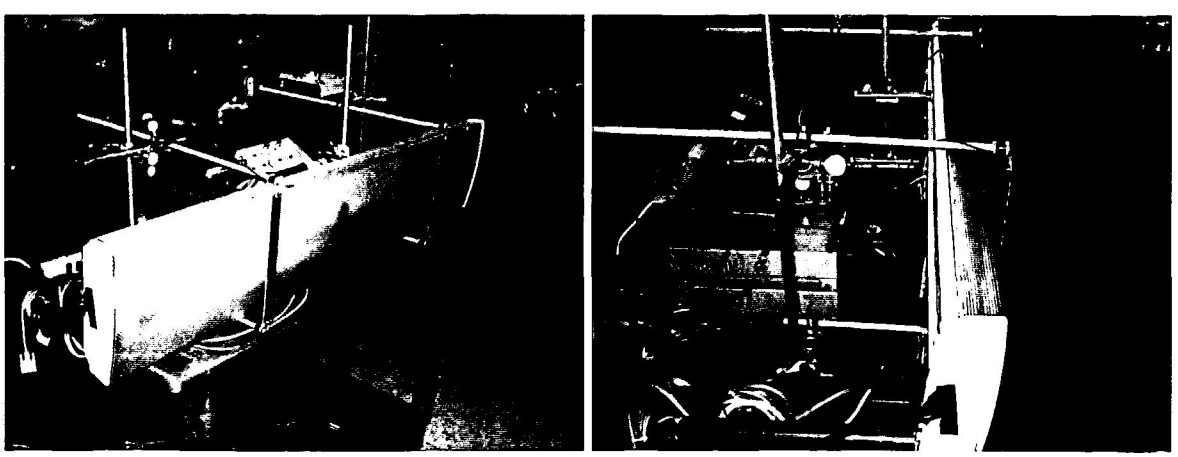

Fig. 1. Photos of the physical experimental lamp sensor configuration.

1-4244-0174-7/06/$20.00 ©2006 IEEE

II. Lumped Capacitor Circuit Model

The diagram shown in Figure 2 illustrates the basic capacitances that couple the lamp, electrodes, and target. The electrodes are placed in front of the lamp, perpendicular to the bulbs and are their respective voltages are labeled e_1 and e_2. The luminaire (backplane) behind the bulbs is grounded and there is a capacitance, C_{bulk} between the target and ground. The capacitance values are discussed below.

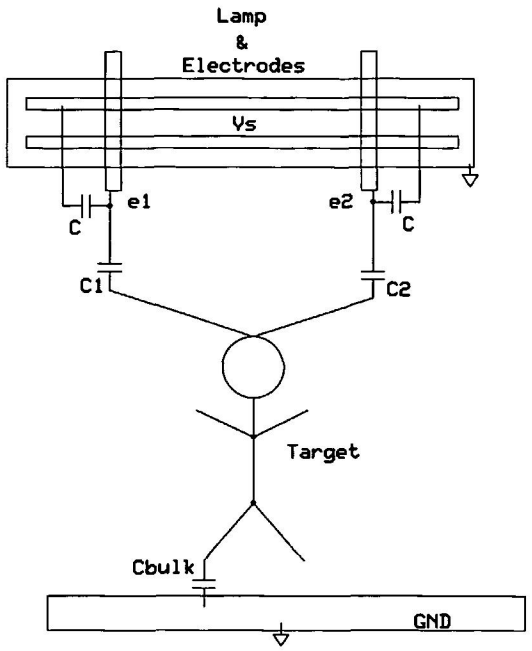

Fig. 2. Pictorial lumped capacitance model

The ac lumped capacitor circuit model shown in Figure 3 of the sensor and target system consists of capacitances between combinations of the lamp, electrodes, target, and ground. The circuit model for a differential measurement between two electrodes is shown. The ac voltage source V_s is measured with respect to ground at the surface of the bulbs and oscillates at 42 kHz, the operating frequency of the lamp ballast.

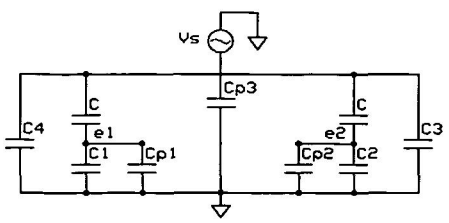

Fig. 3. Ac lumped capacitor circuit model

C_1 and C_2, which are the capacitances we want to measure, couple the electrodes to the target. C_{p1} and C_{p2} are parasitic capacitances between the electrodes and any incremental ground or fixed potential. This includes the capacitances between the electrodes and the luminaire and the earth ground as well as the coaxial shield capacitance for the cables that are connected to the electrodes. C is the same for both electrodes and is the capacitance between the electrodes and the lamp. C_3 and C_4 are the capacitances between the lamp and the target. C_{p3} is the parasitic capacitance between the lamp and any incremental ground. The capacitance, C_{bulk} from Figure 2 between the target and ground is large in comparison to the other capacitances in the system. Therefore it leads to negligible impedance at the operating frequency and the circuit in Figure 3 is shown grounded. Nominally, C_{bulk} is on the order of tens of picofarads (pF), while all the other capacitances in Figure 2 are on the order of 1 pF.

III. Circuit Design and Signal Conditioning

The lumped circuit model leads to a capacitive bridge, more easily seen in Figure 6. The advantage of the capacitive bridge is that the maximum gain is not limited by the dynamic range of the signal conditioning circuitry. If the bridge is nulled, or the values of C match each other and C_1 and C_2 match each other with no target under the lamp, the differential output voltage of the bridge is nulled. Then, the gain can be increased to see small deviations in C_1 and C_2 without saturating the signal conditioning circuitry.

The signal conditioning circuitry for the capacitive bridge requires a differential measurement between the nodes labeled e_1 and e_2. The front-end amplifier is implemented as a fully differential transimpedance amplifier. A simplified schematic of the transimpedance front-end amplifier is shown in Figure 5. The inputs are JFET buffered for higher input impedance and the transimpedance is nominally 1 MΩ. The Common Mode Rejection Ratio (CMRR) of the front-end is bounded by the matching between the feedback transimpedance resistors, which have a rated tolerance of 0.1%. The front-end is compensated with feedback capacitors to limit the gain above the signal frequency and to shape the frequency response of the bridge and front-end as a bandpass.

The lamp and ac bridge are treated as an amplitude modulation system: the high frequency bulb signal is modulated by low frequency disturbances in the electric field below the lamp. A synchronous detection system shown in Figure 4 is implemented to extract the bulb signal.

To generate the synchronous signal or clock signal, a separate electrode is placed against one of the bulbs. This electrode is the input to a single-ended transimpedance amplifier and then squared up with a low-noise comparator. The multiplication between the output of the front-end and the clock signal is performed with a fully differential switch multiplier. After the multiplier, the signal has been demodulated and a low-pass filter is added to limit the bandwidth of the signal to 800 Hz before the input to the analog-to-digital-converter (ADC). The ADC digitally reduces the bandwidth of the signal further and filters integer multiples of 60 Hz pickup before transferring data to a PC.

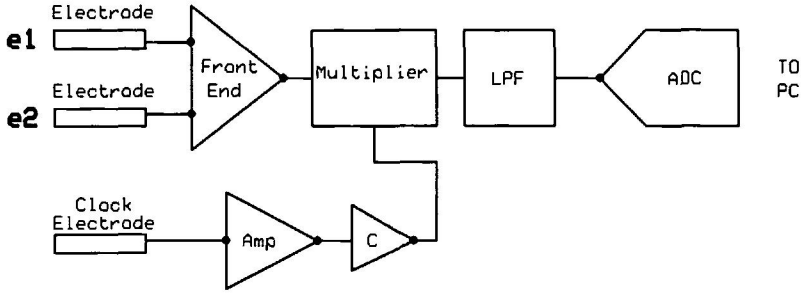

Fig. 4. Block diagram for synchronous detection signal conditioning circuitry

IV. Calculated Response and Noise Floor

To calculate the response of the system to a target, the differential output voltage from the front-end amplifier shown in the block diagram of Figure 4 is calculated. A simplified schematic of the front-end amplifier connected to the measurement electrodes is shown in Figure 5.

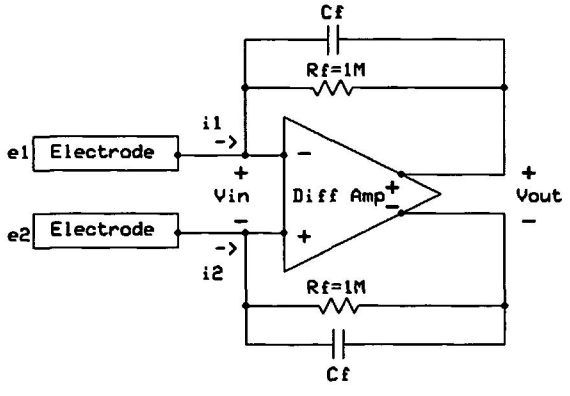

Fig. 5. Simplified schematic of the transimpedance front-end amplifier

The front-end amplifier is a fully-differential transimpedance amplifier. A fully-differential transimpedance amplifier takes a differential current at its input and converts it to a differential output voltage. The differential output voltage is

$$V_{od} = i_{id} Z \tag{1}$$

where i_{id} is the differential input current and Z is the differential transimpedance. The differential transimpedance is set by the feedback impedance and is nominally equal to the value of the feedback resistors labeled R_f, 1 MΩ. The feedback capacitors labeled C_f limit the high frequency gain as explained in Section III. The output voltage of the amplifier is a differential voltage, which is the product of the differential input current and the transimpedance. The negative feedback configuration of the transimpedance amplifier causes the amplifier to fix its differential input voltage, labeled v_{in} to 0 V. It does this by drawing currents so that i_1 and i_2 are equal and opposite. Therefore the front-end amplifier effectively sets the node voltages in the lumped capacitor circuit model of Figure 3, nodes e_1 and e_2, to the same potential. To derive the output voltage of the front-end, the differential current that would pass through a short circuit from node e_1 to e_2 in response to a deviation in C_1 or C_2 is calculated. Finally, the differential current through the effective short circuit is multiplied by the differential transimpedance of the front-end. With the nodes e_1 and e_2 shorted, the ac lumped-capacitor circuit model of Figure 3 reduces to the circuit in Figure 6.

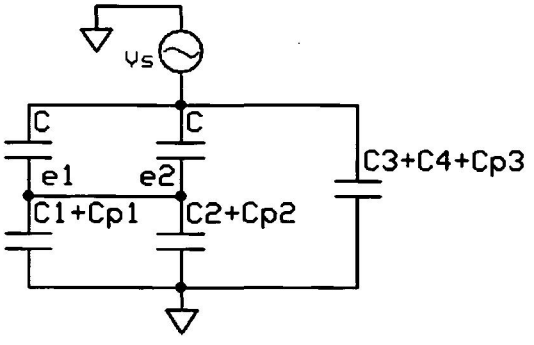

Fig. 6. Reduced lumped capacitor circuit model with effective short

Calculating the product of the differential current and the differential transimpedance leads to the differential output voltage,

$$V_{od} = \frac{2CZ\omega V_s(C_1 + C_{p1} - C_2 - C_{p2})}{C_{p1} + C_{p2} + 2C + C_1 + C_2}. \tag{2}$$

where ω is the signal frequency in radians per second (rps); V_s is the AC voltage at the surface of the bulbs; Z is the differential transimpedance of the front-end.

If the bridge is nulled with no target then for all cases,

$$C_p = C_{p1} = C_{p2} \tag{3}$$

and the parasitic capacitances vanish from the numerator so that the output voltage is

$$V_{od} = \frac{2CZ\omega V_s(C_1 - C_2)}{2C_p + 2C + C_1 + C_2}. \tag{4}$$

Note that in the case where there is no target, (or the target is perfectly centered between the two electrodes)

$$C_1 = C_2 \tag{5}$$

and

$$V_{od} = 0. \tag{6}$$

None of the capacitances C_{p3}, C_3 nor C_4 appear in (4). Also, any capacitance between the two electrodes does not appear in (4) because it is shorted when calculating the differential output voltage from the front-end. The capacitances that do appear in (4) vary for electrode configurations and ranges to the target. Nominal values for these capacitances for a 10 ft. range to the target and 5 in. between the electrodes and the lamp are,

$$C_1, C_2 \approx 200 \text{ f}F$$
$$C \approx 1 \text{ p}F$$
$$C_p \approx 60 \text{ p}F$$

These capacitance values were obtained using the finite-element modeling software, *FastModel*.

The actual response depends on the electrode configuration, which consists of the spacing between the electrodes and the depth between the electrodes and the lamp (electrode depth).

Intuitively, a wider spacing between the electrodes should allow for a longer maximum detection range. This is so because a differential measurement between the two electrodes becomes less significant as the length scale of their separation decreases relative to the length scale of the detection range. This is verified by the plots and will be verified by the data in Section VI. A parallel plate capacitance approximation to the target was used to determine how the response changes as the spacing is varied. Figure 7 shows logarithmic plots of the approximate calculated differential output voltage vs. range for 10 different electrode spacings. The electrode spacing increases moving away from the origin. The spacings vary from 4.8 to 48 inches. The depth between electrodes and the lamp is 5 inches. The reason for plotting the output voltage in ac rms Volts will be clear in Section VI, but a logarithmic plot is used to show the wide dynamic range of the output response over the 10 ft. range.

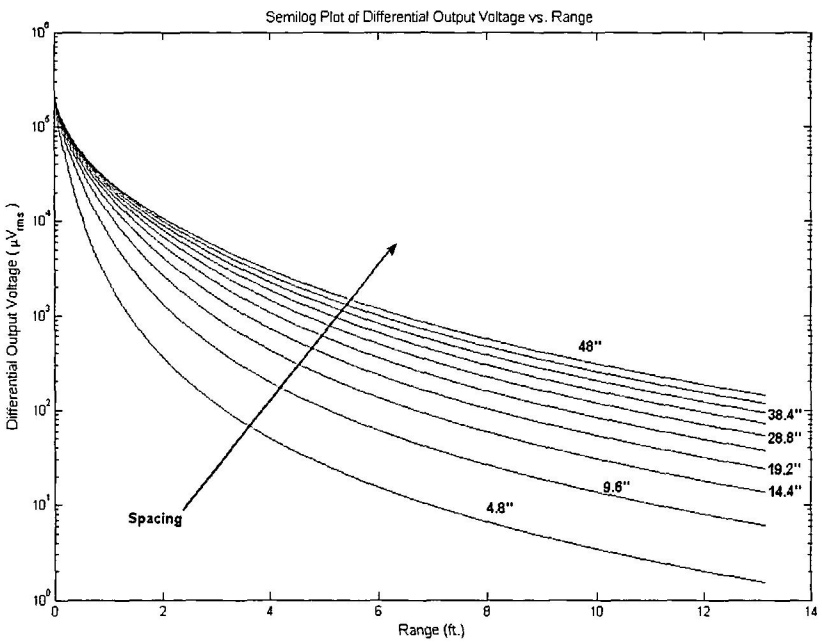

Fig. 7. Calculated Logarithmic Plots of Differential Output Voltage vs. Range for Varying Electrode Spacings. The depth between the electrodes and the lamp is fixed at 5 in. The spacing between the electrodes increases away from the origin in 4.8 in. increments.

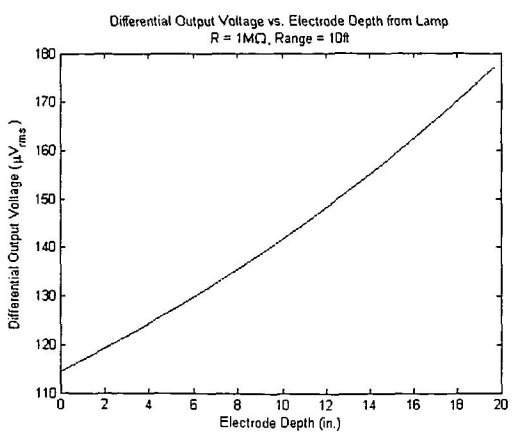

Fig. 8. Differential Output Voltage vs. Electrode Depth from lamp.

Also intuitively, a greater depth between the electrodes and the lamp allows for a longer detection range. This is again because the length scale of the separation becomes more comparable to the length scale of the detection range. Figure 8 shows a plot of the differential output voltage vs. electrode depth from the lamp for a 10 ft. detection and a fixed spacing of 28 in. between the electrodes. These plots can be used to determine how the electrodes should be configured for maximum detection range. For maximum detection range, the electrodes should be spaced as far apart as possible and as far away from the lamp as possible. These plots

can also be used to determine how the electrodes should be spaced to *limit* the maximum detection range. As mentioned in Section I, the lamp sensor could potentially be used to detect metallic objects on a person. One way that this could be done would be to compare the measurements obtained to the measurements that would be expected for a typical human target with no metallic objects in possession. Then, varying the maximum detection range by switching between electrode configurations and taking measurements for each configuration would implement a vertical scanning capability. An anomaly in the dielectric or conductive makeup of the target would be reported as a dramatic difference between the actual measurement and the expected measurement for a specific electrode configuration. Using the vertical scanning technique, the vertical position of the anomaly on the target can likely be deduced. The vertical scanning capability is one example of a potential application of the capacitive lamp sensor that we are pursuing.

Ultimately, the detection range is determined by the signal-to-noise-ratio (SNR). Measurements show that the noise floor of the lamp sensor system is dominated by differential noise from the fluorescent bulbs and ballast. Because the coupling between the electrodes and the bulbs varies with the electrode configuration, the noise floor is a function of the electrode configuration. To quantify total output noise, the output bandwidth must be specified. For the ADC sample rate of 13 samples per second (sps), the effective output bandwidth is approximately,

$$BW \approx 10 \text{ Hz} \tag{7}$$

Then, the significant noise sources add in quadrature as follows:

TABLE I
SIGNIFICANT NOISE SOURCES

Source	Noise (μV_{rms})
Front-End Amplifier	1
Band-Gap Reference for ADC	5
Bulbs and Ballast	50 – 100
Total	50.3 – 100.1

The front-end contributes $1\mu V_{rms}$ noise. The band-gap reference used as a reference for the ADC contributes $5\mu V_{rms}$ of noise. The bulb and ballast contribute approximately $50 - 100\mu V_{rms}$ of noise depending on the electrode configuration. The contribution of each noise source was determined by measuring the total noise as the $V_{AC,rms}$ at the output or with the use of a spectrum analyzer.

The noise measurements were checked for consistency against calculations. The total output voltage noise of the bandgap reference can be found in the data sheet for that particular part, the Linear Technology LT1236. The noise that was measured agreed with the noise level in the data sheet [4].

The total differential output voltage noise from the front-end amplifier can be calculated as follows. The differential input-referred current noise multiplies the differential transimpedance and the feedback transimpedance resistors add their own noise:

$$v_{ontotd} = \sqrt{2(i_{in}^2 Z^2 + 4kTZ)}\sqrt{BW}. \tag{8}$$

in which, i_{in} is the input-referred current noise in rms Amperes per root Hertz ($A_{rms}/\sqrt{Hz}$), k is Boltzmann's constant ($m^2kg/s^2/K$), T is the absolute temperature in Kelvin (K), Z is the differential transimpedance in Ohms Ω, and BW is the bandwidth after the ADC in Hertz (Hz).

From the data sheet for the JFET input buffers [5] at the inputs to the front-end amplifier, the input-referred current noise is,

$$i_{in} = 5\frac{fA}{\sqrt{Hz}}. \tag{9}$$

and, Boltzmann's constant is $k = 1.38^{-23} m^2 kg/s^2 K$. The ambient temperature is taken to be $T \approx 300K$. The transimpedance is $Z = 1\ M\Omega$ and the output bandwidth is $BW \approx 10Hz$. Inserting these values into (8) results in

$$v_{ontotd} = 0.57\ \mu V_{rms}, \tag{10}$$

which agrees well with the measurements above.

The maximum detection range for each electrode configuration (and a specific confidence level (see Section VI)) is determined by the range at which the response becomes comparable to the noise level.

V. ELECTRODE AND LAMP CONFIGURATION

The physical configuration of the lamp is shown in Figure 1. The lamp is suspended from the back side with a metallic support and the electrodes are placed in front of the lamp suspended by wooden (nonconducting) supports.

The lamp uses two Philips Universal 48 in. fluorescent bulbs and a 42kHz Sylvania Electronic Ballast, both commercial-off-the-shelf. Two relatively insignificant, but important electrical modifications are made to the lamp. The first is that the ground connection from the ballast to the backplane is taken out of the back of the lamp and referenced as the ground for the lamp sensor electronics as well. This creates a global dc ground reference. It eliminates some inconsistency and drift or noise due to parasitic coupling between the bulbs and the backplane, and the electrodes and the backplane.

The second modification is that the bulbs are run 180° out of phase or opposite to each other. This is achieved by reversing the ballast connections to one of the bulbs. This modification is necessary to create a symmetrical summed voltage distribution along the length of the bulbs. Then, the sum of the potential across the two bulbs at a point along their length, which is obtained with the metallic electrodes, is equal to the sum of the potentials at the point symmetrical to it about the center of the bulbs (at the other electrode). Note that the bulb voltage distribution along the length of the bulb is asymmetric about the center and nonlinear as shown in Figure 9 taken from Dakin [1].

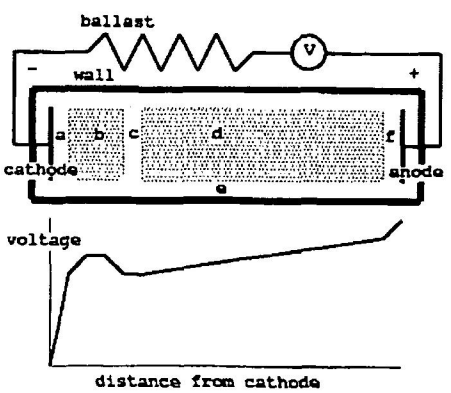

Fig. 9. A plot of the fluorescent bulb voltage profile.[1]

If the voltage distribution along the length of the bulb were symmetric about the center, then the sum of the potentials at all points along the length of the bulbs with the bulbs run out-of-phase would be 0 V. If the bulb voltage distribution along the length of the bulb were symmetric and the bulbs were run in-phase, then the sum of the potentials at a point along the length would be *antisymmetric* about the center. With the voltage distribution asymmetric about the center and the bulbs run in-phase, the sum of the potential at a point along the length would be *asymmetric*.

The physical configuration of the lamp is important in achieving good performance. To null the bridge and have good CMRR, the electrode position in front of the lamp must be well-controlled. If the CMRR of the front-end is bounded by the 0.1% matching of the feedback resistors, then the capacitance at the input of the front-end must be matched better than 0.1% to not significantly degrade the CMRR. Therefore the depth from the lamp to the two electrodes must be matched better than 0.1%.

For instance, for a general parallel plate capacitance,

$$C(x) = \frac{\epsilon A}{x} \tag{11}$$

where, ϵ is the permittivity of the material between the plates, A is the cross-sectional area of the plates and x is the separation between the plates.

The Taylor series approximation to deviations in x is,

$$C(x) \approx C(x_0) + \frac{d}{dx}C(x)|_{x=x_0}(x - x_0) \tag{12}$$

And the second term

$$\frac{d}{dx}C(x)|_{x=x_0}(x - x_0) = -\frac{\epsilon A}{x_0^2}(x - x_0) \approx \Delta C \tag{13}$$

but,

$$\Delta C < -10^{-3}C(x_0) = -10^{-3}\frac{\epsilon A}{x_0} \tag{14}$$

so, from (13) and (14),

$$x - x_0 = \Delta x < 10^{-3}x_0. \tag{15}$$

The electrodes are nulled by adjusting the electrode depth from the lamp while watching the output voltage approach $0V$. The electrodes must be on-axis: that is, they must couple to the two bulbs equally. Finally, the standard lamp cover provides a still-air environment for the bulbs, eliminating some random differential-mode bulb voltage variations due to thermal convection at the surface of the bulbs.

VI. Lamp Sensor Prototype Experimental Data

Data was taken on the prototype lamp sensor and recorded for a person walking below the lamp for varying range and electrode configurations. Each electrode configuration consisted of an electrode spacing and depth.

Because a differential measurement is taken from the capacitive bridge, a target in front of one electrode has the opposite effect of a target in front of the other electrode. Therefore, a target passing by under the lamp should result in a time-domain output voltage waveform that begins at the nulled voltage, deviates in one direction, then returns to the nulled voltage, crosses it and then deviates in the other direction before returning to the nulled voltage again. A typical time-domain waveform of a person walking 6 ft. under the lamp is shown in Figure 10. The data in Figure 10 was collected from the output of the circuit shown in the block diagram of Figure 4 and plotted in MATLAB.

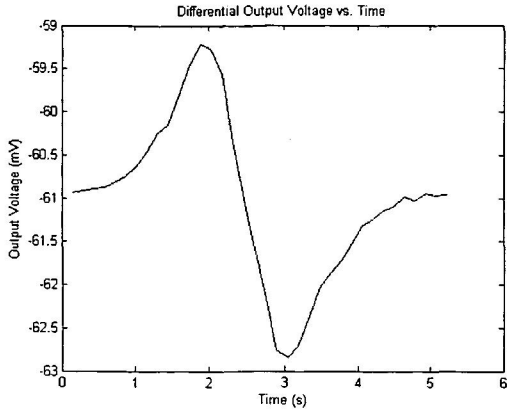

Fig. 10. A typical output voltage waveform of a 6 ft. detection.

The key performance metric is the signal-to-noise-ratio (SNR), which is constrained by the rms noise voltage at the output of the lamp sensor. Therefore, the ac rms voltage ($V_{ac,rms}$) of the collected data sample is measured to determine the strength of the detection and to compare it to the noise floor. As previously stated, the noise floor is roughly $50-100$ μV_{rms} depending on the electrode configuration. $V_{ac,rms}$ of the 6 ft. detection above is 1.05 mV_{rms}, a strong detection. A 10 ft. detection is shown in Figure 11. Since 10 ft. is the current limit of the detection range, noise variations are clearly seen in this plot. $V_{ac,rms}$ for this detection is only 80 μV_{rms}, but clearly in this electrode configuration less than 80 μV_{rms} noise appears at the output.

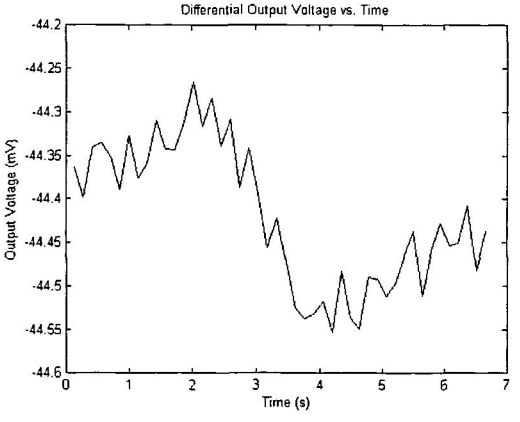

Fig. 11. A 10 ft. detection showing noise variations.

Data was taken in 20 different electrode configurations. Each configuration consisted of an electrode spacing and depth from the lamp. Each sample consisted of one pass of a target person walking under the lamp. The metric for each sample was the ac rms output voltage ($V_{ac,rms}$). For each configuration, 10 control samples were taken with no target passing under the lamp. Then for each range in each electrode configuration, 5 samples were taken of a target person passing under the lamp. The range is defined as the distance between the lamp and the closest edge of the target. A Z-test [2] in MATLAB was performed on the data comparing each 5-sample set of data to the control set for that configuration. The chosen detection rule is that the sample set must demonstrate a mean $V_{ac,rms}$ larger than that of the control sample set with a confidence level of 99% or

better. The data is shown in Table II at the boundary of the detection rule. The range varies along the columns. The configuration varies along the rows. Each configuration is labeled as an electrode spacing (the distance between the two electrodes) and and electrode depth (the distance from the lamp to the electrodes).

The Z-test measures the statistical likelihood that the means of two gaussian-distributed random variables are different based on the mean and variance calculated from sample sets of the two variables. We introduce the *p-value* to quantify the confidence level of detection where, p is the probability that the means of the two sample sets are equal. Thus a higher *p-value* signifies a higher probability that there is no detection. Therefore, the confidence level α that there has been a detection is defined as:

$$\alpha = 1 - p. \tag{16}$$

or, the percent confidence that there has been a detection is

$$P_C = 100\alpha. \tag{17}$$

So, for example the percent confidence for the 10 ft. range in the configuration with the electrodes 2 in. from the lamp and 28 in. apart (2x28) is,

$$P_C = 100(1 - p) = 100(1 - 0.027) = 97.3\% \tag{18}$$

and it is rejected as a detection based on the 99% confidence level rule.

In the table, a *p-value* of 0 means nearly zero, so that the confidence level is negligibly less than 100%. "N/A" means that a range lesser than the current range has shown questionable detection and this range is not considered. Thus the *p-values* for sample sets up to the first sample set when $p > 0.01$ or $100\alpha < 99\%$ are shown in the table. Also, all *p-values* at the detection range boundary that are less than 10^{-7} are listed as $< 10^{-7}$. The noise floor is listed with each configuration. It is calculated as the mean of the ($V_{ac,rms}$) measurements for the 10 control samples taken for that configuration.

TABLE II

DETECTION DATA $p - values$ FOR VARIOUS ELECTRODE CONFIGURATIONS AT THE LIMIT OF THE DETECTION RANGE.

		p-values					
Spacing(in.)	Depth(in.)	7ft.	8ft.	9ft.	10ft.	11ft.	Noise Floor ($\mu V_{ac,rms}$)
44	5	0	0	0	2.53×10^{-4}	0.328	54.5
	4	0	0	4.63×10^{-7}	0.0165	N/A	65.1
	3	0	0	0	4.85×10^{-6}	0.661	98.9
	2	0	$< 10^{-7}$	0.0426	N/A	N/A	168.5
38	5	0	0	3.05×10^{-5}	0.0240	N/A	61.8
	4	0	0	4.93×10^{-5}	0.865	N/A	67.3
	3	0	0	$< 10^{-7}$	0.133	N/A	62.7
	2	0	0	0.00200	0.0160	N/A	74.0
28	5	0	0	0	$< 10^{-7}$	0.306	45.2
	4	0	0	1.19×10^{-4}	0.676	N/A	70.7
	3	0	0	$< 10^{-7}$	0.884	N/A	52.3
	2	0	2.62×10^{-5}	0.00100	0.0270	N/A	65.3
19	5	0	$< 10^{-7}$	0.382	N/A	N/A	55.4
	4	0	0	$< 10^{-7}$	0.126	N/A	41.6
	3	0	$< 10^{-7}$	0.0120	N/A	N/A	45.4
	2	0	0	1.01×10^{-5}	0.0340	N/A	42.2
15	5	0	$< 10^{-7}$	0.0360	N/A	N/A	40.9
	4	$< 10^{-7}$	0.0210	N/A	N/A	N/A	51.5
	3	0	$< 10^{-7}$	0.0640	N/A	N/A	49.9
	2	$< 10^{-7}$	0.0120	N/A	N/A	N/A	57.2

The data demonstrates detection ranges from 7 ft. to 10 ft. depending on the electrode configuration. There is a trend as the electrodes become closer to the lamp and more closely spaced for the detection range to decrease. These results agree with the calculated response and the effect of the electrode configuration discussed in Section IV.

VII. CONCLUSIONS

This paper has shown how a fluorescent lamp as a capacitive sensor can be used as a detection device. The lumped capacitor model led to signal conditioning circuitry for a synchronous amplitude modulation detection system. Calculated responses compared to noise levels led to practical detection ranges that were validated experimentally.

The lamp sensor system shows potential for security detection and tracking applications. Further work will attempt to extend the detection range of the lamp sensor. It will also investigate the vertical scanning technique described in section IV and the potential to use the lamp sensor as a metal and dangerous materials detector in public spaces. Finally, further work will investigate the next step in exploiting the fluorescent lamp infrastructure for security applications.

VIII. ACKNOWLEDGEMENTS

We would like to acknowledge the generous support for this research by the United States Department of Justice, the Grainger Foundation, and the Center for Materials Science and Engineering at MIT.

REFERENCES

[1] James T. Dakin. "Nonequilibrium Lighting Plasmas". *IEEE Transactions on Plasma Science*, Vol. 19, No. 6, 1999.

[2] C.-C. Wang and R.J.-W. Chen. "Three Modified Dependency-tests for Software Failures". *IEEE Proceedings on Reliability and Maintainability*, 2002.

[3] C. L. Chua, R.L. Thornton, D.W. Treat, V.K. Yang, and C. C. Dunnrowicz. "Indium Tin Oxide Transparent Electrodes for Broad-Area Top-Emitting Vertical-Cavity Lasers". *IEEE Photonics Technology Letters*, Vol. 9, No. 5, 1997.

[4] "(LT1236) data sheet". Linear Technology. Milpitas, CA, USA.

[5] "(AD8610) data sheet". Analog Devices. Norwood, MA, USA.

IX. VITAE

John Cooley is currently a Doctoral student at the Massachusetts Institute of Technology studying Electrical Engineering. He received the S.B. degree in Electrical Engineering and the S.B. degree in Physics in 2005 at MIT. His research interests include electromagnetics, capacitive sensors, and low-noise analog electronics design.

Al-Thaddeus Avestruz is currently a Ph.D candidate in Electrical Engineering at the Massachusetts Institute of Technology. He received his S.B. in Physics in 1994 and his S.M. and Engineer's degrees in 2006, also at MIT. He has worked for a number of companies including Teradyne Corporation, Diversified Technologies and Talking lights, LLC. His research interests include circuit design, sensors, electro-magnetics and electrical machinery, embedded systems, alternative energy and power electronics.

Dr. Steven B. Leeb received S.B., S.M., E.E. and Ph.D. degrees from MIT. He has been a member of the MIT faculty in the Department of Electrical Engineering and Computer Science since 1993. He serves as a professor in the Laboratory for Electromagnetic and Electronic Systems. He is concerned with the design, development, maintenance, and security processes for all kinds of machinery with electrical actuators, sensors, or power electronic drives.